Contrib Mineral Petrol (2001) 142: 15–26
DOI 10.1007/s004100100277

R. Milke · M. Wiedenbeck · W. Heinrich

Grain boundary diffusion of Si, Mg, and O in enstatite reaction rims: a SIMS study using isotopically doped reactants

Received: 9 January 2001 / Accepted: 4 May 2001 / Published online: 3 July 2001

Abstract Diffusion-controlled growth rates of polycrystalline enstatite reaction rims between forsterite and quartz were determined at 1,000 °C and 1 GPa in presence of traces of water. Iron-free, pure synthetic forsterite with normal oxygen and silicon isotopic compositions and quartz extremely enriched in ^{18}O and ^{29}Si were used as reactants. The relative mobility of ^{18}O and ^{29}Si in reactants and rims were determined by SIMS step scanning. The morphology of the rim shows that enstatite grows by a direct replacement of forsterite. Rim growth is modelled within a mass-conserving reference frame that implies advancement of reaction fronts from the initial forsterite–quartz interface in both directions. The isotopic compositions at the two reaction interfaces are controlled by the partial reactions $Mg_2SiO_4 = 0.5\,Mg_2Si_2O_6 + MgO$ at the forsterite–enstatite, and $MgO + SiO_2 = 0.5\,Mg_2Si_2O_6$ at the enstatite–quartz interface, implying that grain boundary diffusion of MgO is rate-controlling. Isotopic profiles show no silicon exchange across the propagating reaction interfaces. This propagation, controlled by MgO diffusion, is faster than the homogenisation of Si by self-diffusion behind the advancing fronts. From this, and using $D^{Vol}_{Si,En}$ at dry conditions from the literature, results a $D'_{Si,En}\delta$ value of 3×10^{-24} m^3 s^{-1} at 1,000 °C. The isotopic profiles for oxygen are more complex. They are interpreted as an interplay between the propagation of the interfaces, the homogenisation of the isotope concentrations by grain boundary self-diffusion of O within the rim, and the isotope exchange across the enstatite–quartz interface, which was open to ^{18}O influx from quartz. Because of overlapping diffusion processes, boundary conditions are unstable and $\acute{D}_{Ox,En}\delta$ cannot be quantified. Using measured rim growth rates, the grain boundary diffusivity $\acute{D}_{MgO}\delta$ of MgO in iron-free enstatite is 8×10^{-22} m^3 s^{-1} at 1,000 °C and 1 GPa. Experiments with San Carlos olivine (fo_{92}) as reactant reveal lower rates by a factor of about 4. Our results show that isotope tracers in rim growth experiments allow identification of the actual interface reactions, recognition of the rate-controlling component and further calculation of $\acute{D}\delta$ values for specific components.

R. Milke (✉) · M. Wiedenbeck · W. Heinrich
GeoForschungsZentrum Potsdam, Telegrafenberg,
Potsdam, Germany
E-mail: rmilke@gfz-potsdam.de
Tel.: +49-0331-2881483
Fax: +49-0331-2881402

Editorial responsibility: J. Hoefs

Introduction

Diffusive transport controls the rates of many chemical and physical processes in rocks. The transport of chemical components is often dominated by grain-boundary diffusion because volume diffusion in most minerals is much slower. Grain-boundary diffusivities have been experimentally determined for a number of chemical components in aggregates of rock-forming minerals. Two different experimental strategies have been applied: the tracer diffusion method uses the self-diffusion of an isotope tracer into a polycrystalline aggregate (e.g. Farver and Yund 1992, 1995a, 1995b, 1996; Farver et al. 1994), whereas the rim growth method uses the diffusion-controlled growth rates of polycrystalline reaction rims between incompatible reactants to determine the kinetics of the underlying diffusion process (Brady 1983; Fisler and Mackwell 1994; Fisler et al. 1997; Liu et al. 1997; Yund 1997; Milke and Heinrich 2000). Whereas tracer diffusion involves the migration of single chemical species, the growth of reaction rims requires transport of several atomic species via coupled diffusion or counter-diffusion in order to maintain stoichiometric and charge balance.

The experimental strategy in rim growth experiments is to use a simple chemical reaction of the type phase I + phase II = rim of phase III. The dependence of the rim thickness on temperature and run duration is measured. The aim is to derive values for the grain-boundary diffusion coefficient (D') of the rate-determining

component times the effective grain-boundary width (δ):

$$D_A^{gb}\delta = dRTX^2 \Big/ \left(\pi\left[\sum (v_\Phi/v_A)\right] c_A V_\Phi \Delta\mu_A t\right) \quad (1)$$

(Yund 1997), where X = thickness, t = time, $\Delta\mu$ = difference of the chemical potential of component A between phase I and II, T = temperature, R = gas constant. All other variables are geometrical and stoichiometrical factors. The crucial point of this strategy is that several components are migrating within the rim, and that different species may have different mobilities. If so, it is difficult to identify the component for which the grain-boundary diffusion coefficient has actually been measured, and the rate-limiting step that controls the overall diffusion process remains unclear. To overcome this, inert markers have been used to preserve the position of the initial interface between the reactants and to draw conclusions on the relative mobilities of different components (e.g. Brindley and Hayami 1965; Fisler and Mackwell 1994; Fisler et al. 1997; Yund 1997). However, experiments with inert markers might be misleading for several reasons, for example when the markers migrate with advancing reaction interfaces. Another approach uses reactants that have been isotopically doped. Using SIMS step scanning the migration of each component can then be traced from both phase boundaries into the developing reaction rim.

Several experimental studies have shown that intracrystalline diffusion in pyroxenes is particularly slow (e.g. Béjina and Jaoul 1996; Dimanov et al. 1996; Edwards and Valley 1998). Grain boundaries in polycrystalline reaction rims of pyroxene therefore provide a pathway for fast chemical transport. Experiments on the growth rates of enstatite produced by the reaction olivine + quartz = enstatite:

$$2\,Mg_{0.92}Fe_{0.08}SiO_4 + SiO_2 = Mg_{1.84}Fe_{0.16}Si_2O_6 \quad (2)$$

at high temperatures and atmospheric to high pressures revealed parabolic growth rate laws, proving that grain boundary diffusion controls rim growth (Fisler et al. 1997; Yund 1997). In this paper, experiments on the reaction forsterite + quartz = enstatite are presented. Iron-free, pure synthetic forsterite with natural oxygen and silicon isotopic compositions and quartz extremely enriched in ^{18}O and ^{29}Si were used as reactants. By step scanning with an ion probe (SIMS) the relative mobility of the isotopes can be defined. We show that the measured isotope diffusion profiles can be reasonably interpreted in terms of the microstructural evolution and the volume change of the proceeding reaction, allowing us to infer the rate-limiting diffusion mechanism.

Experimental and analytical methods

Four experiments were performed, three with isotopically undoped, and one with isotopically doped reactants, using a conventional piston-cylinder apparatus with fluorite as the pressure cell medium. About 25 mg of starting material were placed into a 10-mm-long and 3-mm-wide Pt capsule with a 0.1-mm wall thickness. Run conditions for all experiments were 1,000 °C and 1 GPa; run durations were between 24 and 50 h. Temperatures were measured with a mantled chromel–alumel thermocouple placed in contact to the central part of the capsules. The error in temperature was about ±10 °C, pressure accuracy was ±30 MPa. Undoped starting materials were either grains of San Carlos olivine ($fo_{92}fa_8$), sieved to 125–200 μm, or iron-free synthetic forsterite (102–200 μm), placed in a fine-grained matrix (20–35 μm) of clear Brazilian quartz. Oxygen fugacity was not buffered in runs with iron-bearing olivine. In all runs except one no water was added to the mixture. Because the reactant powder was not dried, a small amount of adsorbed water was probably present during all runs. The amount of adsorbed water can be estimated based on BET surface area measurements of crushed quartz in various grain sizes assuming a typical adsorption layer thickness of 5 molecular units (Parks 1990). The approximate water content in the undried experiments is estimated to be about 0.01 wt%. One run was performed with the addition of 0.4 wt% water.

In the isotope tracer experiment about 5 mg chemically pure forsterite (102–200 μm) was dispersed in 20 mg isotopically doped quartz. There was no addition of water and no drying before the capsule was sealed. The quartz had been strongly enriched in ^{29}Si and ^{18}O. It was prepared by hydrothermal equilibration of synthetic SiO_2 consisting of 94.3 mol% $^{29}SiO_2(^{29}Si/(^{28}Si + ^{29}Si) = 0.95$; Cambridge Isotope Laboratories, Andover, MA) with water containing 94.4 mol% $H_2{}^{18}O$ (Promochem). The equilibration between quartz and water was performed in hydrothermal anneals for 120 h using conventional cold-seal vessels. The Pt capsules containing quartz enriched in ^{29}Si and water enriched in ^{18}O were placed in such a way that there was thermal gradient of about 70 °C along the 5-cm-long capsules. The $^{29}SiO_2$ powder was initially placed at the hot end of the capsule that was heated to 700 °C. Dissolution and subsequent precipitation at the cooler end of the capsule at about 630 °C ensured isotopic equilibration between quartz and fluid. Pressure was 500 MPa at the first day of the hydrothermal runs and was then reduced to 100 MPa. From mass balance considerations, the $^{18}O/(^{18}O + ^{16}O)$-ratio of quartz in equilibrium with fluid is 0.64. Mass spectrometric analyses of this quartz powder, measured at University of Göttingen, revealed a value of 0.60 ± 0.04 (Klaus Simon, personal communication 1999). The mean grain size of the isotopically doped quartz was about 25 μm. Iron-free, synthetic forsterite had a natural ^{29}Si and ^{18}O composition with $^{29}Si/(^{28}Si + ^{29}Si) = 0.05$ and $^{18}O/(^{18}O + ^{16}O) = 0.002$. Thus, the reactants had completely different isotopic compositions for both silicon and oxygen isotopes.

After the experiments the capsules were embedded in epoxy and polished to make either polished sections or petrographic thin sections. Rim width measurements were determined from back-scattered electron images (Fig. 1) and from transmitted light micrographs of the thin sections.

We used a Cameca ims 6f ion microprobe to conduct point profiles from forsterite across the enstatite boundary layer into the quartz matrix. Prior to analysis the 'best' locations on the polished sample surface were identified by BSE imaging. The sample was then cleaned in ethanol, dried in an oven at 75 °C and coated with a conductive gold film. For the SIMS measurements we used a 10-kV $^{133}Cs^+$ primary beam with an intensity of 7 pA. Based on a manual scan across a Cu grid wire we determined that our beam width was < 2 μm. Positive secondary ions were extracted through a 7.5-kV extraction potential to which no offset was applied. We were unable to detect the presence of significant isobaric interferences, and hence we operated our mass spectrometer at low mass resolution ($M/\Delta M \approx 350$). Our secondary ion optics employed a 50-V energy bandpass, a 150-μm contrast aperture and an 100-μm field aperture, equivalent to a 5-μm diameter field of view. Data collection, employing an ETP ion pulse counter, involved magnet switching through the sequence ^1H, ^{16}O, ^{18}O, ^{24}Mg, ^{28}Si and ^{29}Si; each species was integrated for 10 s. Each measurement spot was automatically pre-sputtered for 10 min followed by the actual analysis consisting of 12 cycles of the peak-stepping sequence. Thus, a single measurement lasted ~25 min, which was followed by a 1-μm step by the stage motors prior to initiating the next spot's pre-burn.

Results

Experimental conditions along with the square of the measured rim thicknesses are given in Table 1. Enstatite is the only reaction product in our experiments, and it always forms polycrystalline rims around forsterite grains. Thus, forsterite is replaced by enstatite. There is no enstatite formation apart from the rims around the forsterite. Within each experiment, the enstatite rims have constant thickness over the entire sample. The two boundaries of the enstatite rims are morphologically different; the forsterite–enstatite interface is always smooth whereas the enstatite–quartz interface is always irregular with numerous enstatite prisms growing into the surrounding quartz crystals (Fig. 1a). Growth of prismatic crystals pointing out of the rim into the quartz matrix is observed in all runs. This is most striking in the experiment with 0.4 wt% water added (Fig. 1b). Many of these crystals are about 20 μm long, in contrast to crystal diameters of about 1 μm within the rim. Where water was added, fluid inclusions are frequently present within the rim and particularly along the enstatite–forsterite interface (Fig. 1b). In experiments without water addition, fluid inclusions are absent.

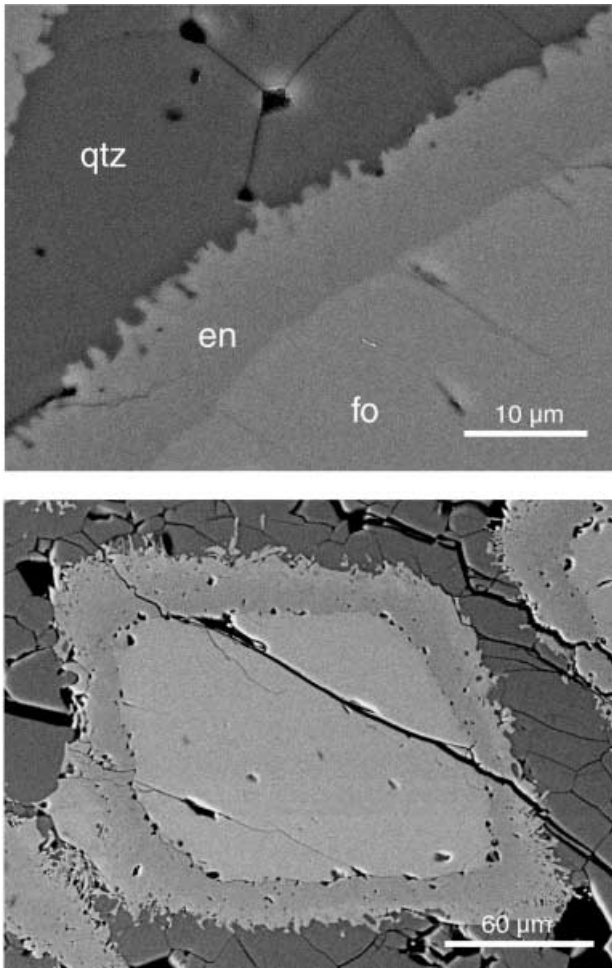

Fig. 1a, b Back-scattered electron images of a polished sample surface showing an enstatite rim between San Carlos olivine ($fo_{92}fa_8$) and quartz. **a** Reaction boundary between forsterite and enstatite is smooth and even. At the quartz–enstatite interface, freely developed enstatite crystals point into the quartz. (Run FQ001, 1,000 °C, 1 GPa, 50 h, no water added). **b** Enstatite rim around San Carlos olivine produced with addition of water. Fluid inclusions are trapped along the enstatite–forsterite interface (Run FQ002, 1,000 °C, 1 GPa, 50 h, 0.4 wt% water added)

Experiments at 1,000 °C and 1 GPa with San Carlos olivine as reactant yielded, under nominally dry conditions, a rim thickness of 8.7 ± 1.5 μm (1σ) after 50 h (Table 1). With 0.4 wt% water added, the rim thickness increased to 15.7 ± 1.9 μm for the same time span. In comparison, experiments with iron-free synthetic forsterite resulted in distinctly wider enstatite rims. Here, under nominally dry conditions, the rim thickness is 15 ± 1.7 μm after 24 h, and 20.3 ± 3.0 μm after 50 h (Table 1). This is in overall agreement with enstatite reaction rim widths produced at similar conditions by Yund (1997), using natural olivine (fo_{92}) as reactant (see discussion below).

In Fig. 2, measured isotope ratio profiles along reaction rims from isotopically doped run FQ004 are depicted for $^{18}O/(^{16}O + ^{18}O)$ and $^{29}Si/(^{28}Si + ^{29}Si)$. Figure 2a represents a 15-μm-wide enstatite rim produced during 24 h, Fig. 2b a 19-μm-wide rim from the same run. The apparently wider rim results from an oblique sectioning effect. Both profiles are very similar, despite their different lengths.

The ^{18}O and the ^{29}Si concentrations show plateau values within quartz and forsterite. These concentration plateaus are connected by smooth concentration gradients across the enstatite rims. The profile of Si appears nearly symmetrical along the rim, whereas the profile of O is not. The concentration plateaus of the $^{29}Si/(^{28}Si + ^{29}Si)$ ratios in both quartz and forsterite are 0.96 and 0.07, respectively, and thus closely represent the initial isotope concentrations of the reactants. Within our spatial resolution of $\sim$2 μm, these ratios are well preserved on either side of the reaction boundary. This suggests that quartz and forsterite remained closed to Si exchange with the enstatite rim. With respect to oxygen, the forsterite plateau is very close to the initial $^{18}O/$

Table 1 Run conditions and squares of measured enstatite rim widths ($\pm 1\sigma$)

Run no.	Olivine	Quartz	Water	T (°C)	P (MPa)	t (h)	x^2 (μm^2)
FQ001	SC olivine	Natural	Not added	1,000	1,000	50	78 ± 28
FQ002	SC olivine	Natural	0.4 wt%	1,000	1,000	50	251 ± 59
FQ003	Synth fo	Natural	Not added	1,000	1,000	50	420 ± 128
FQ004	Synth fo	Doped	Not added	1,000	1,000	24	228 ± 59

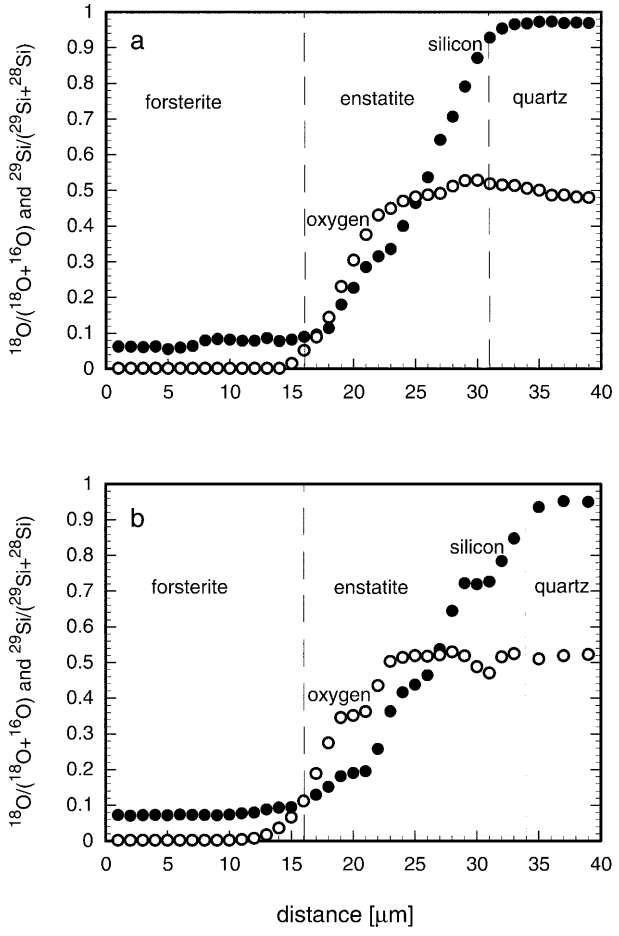

Fig. 2a, b Step scanned $^{29}Si/(^{28}Si+^{29}Si)$ and $^{18}O/(^{16}O+^{18}O)$ profiles from iron-free forsterite across the enstatite rim into isotopically doped quartz. *Dashed lines* indicate the position of the forsterite–enstatite and enstatite–quartz interfaces. Both profiles are from sample FQ004. The apparently wider rim in **b** results from an oblique sectioning effect. *Filled circles* $^{29}Si/(^{28}Si + ^{29}Si)$ ratios; *open circles* $^{18}O/(^{16}O + ^{18}O)$ ratios

($^{16}O+^{18}O$) of 0.002. Only the outermost few micrometers show a slight increase in ^{18}O concentration. The extent of this increase is, however, within the range of the spatial resolution of the SIMS. If so, forsterite did not see ^{18}O from quartz. By contrast, the $^{18}O/(^{16}O+^{18}O)$ ratio of 0.52 measured in quartz is significantly lower than the initial ratio of 0.60, and this low value was measured 10 μm from the enstatite–quartz interface into the quartz grains. Obviously, quartz did see isotopically light oxygen from the forsterite reactant, implying that quartz was open to oxygen exchange with the enstatite rim. A second striking point is that the oxygen isotope signature of quartz, high in ^{18}O, extends far into the enstatite rim. The observed oxygen isotope ratio remains high across much of the rim and drops to the initial ratio of forsterite near the forsterite–enstatite boundary. The shapes of the silicon and oxygen isotope concentration profiles are different. It is clear that this is caused by the contrast between the migration behaviour of oxygen and silicon during rim formation.

In Fig. 2b, the isotope profiles appear somewhat irregular at distances of 20 to 22 μm and 30 to 32 μm. This is because the measurement spots included micropores resulting in an apparent decrease in both ^{29}Si and ^{18}O concentrations. Such inconsistencies are easily identified because both the ^{29}Si and ^{18}O concentrations are affected in the same manner.

Discussion

Direction of rim growth: the volume argument

In principle, the enstatite rims could grow from the initial forsterite–quartz interface either in one direction or towards both sides. The different morphologies of the enstatite–quartz and enstatite–forsterite interfaces indicate two distinct partial reactions that are controlled by distinct mechanisms. Smooth interfaces occurring between enstatite and forsterite are typical for diffusion-controlled reactions. In contrast, irregular interfaces with well-developed crystal faces, as seen at the enstatite–quartz boundary, indicate interface-controlled kinetics (e.g. Berner 1978). Overall rim growth results from the partial reactions at the two interfaces. The overall growth rate follows a parabolic rate law (Yund 1997; see also runs FQ003 and 004, Table 1) and is therefore controlled by diffusion of a single diffusing component through the reaction rim. Morphology shows that only the partial reaction at the enstatite–forsterite interface is diffusion controlled. This, in turn, suggests that the overall rate of diffusive transport through the rim is regulated by that component that is produced or consumed at the forsterite–enstatite interface during reaction.

At experimental conditions, the volume change ΔV of the reaction forsterite + quartz = enstatite is about –6%. Obviously, compaction of the quartz matrix occurred simultaneously to rim growth. This compaction allowed growth of large enstatite crystals into the quartz matrix (Fig. 1a, b). Because no open gaps were observed after reaction, significant quartz recrystallisation must have occurred around the large enstatite needles.

We showed above that enstatite growth involves the direct replacement of forsterite. A forsterite grain reacting with the surrounding quartz matrix represents a closed system, where the spatial shift of the two rim boundaries away from the initial forsterite–quartz interface is expressed within a mass-conserving reference frame. The volume proportions of the reactants and products are given by reaction stoichiometry. In our reaction, the volume of the consumed part of forsterite is 69.7% the volume of the enstatite that is formed at the same time. Given direct replacement of forsterite by enstatite, it follows that maximally 69.7 vol% of enstatite grew inwards, and at least 30.3 vol% grew outwards from the initial forsterite–quartz interface. The position of the initial interface can be calculated by

$$d_{inw} = \frac{1}{2}\left(\left[d_i^3 + X\left(d_o^3 - d_i^3\right)\right]^{1/3} - d_i\right) \quad (3)$$

with d_i = inner width of the reaction rim, d_o = outer width of the reaction rim, where $X = \frac{mV_{mol,forsterite}}{nV_{mol,enstatite}}$ and m,n are the number of moles of forsterite and enstatite, respectively (Fig. 3). If reaction rims are thin compared with the entire grain size, the widths of the inwards and outwards grown parts approach the inwards and outwards grown volumes, so that

$$\frac{d_{inw}}{d_{total}} \rightarrow \frac{mV_{mol,react}}{nV_{mol,prod}} \quad (4)$$

Crucial for identifying the direction of rim growth is establishing the initial position of the interface between incompatible reactants. Hence, it is essential that we consider the volume proportions of both the reacting and the generated phases.

Restrictions on the rate-limiting diffusion process

In a three-component system the rate-limiting diffusion process might be dominated by the diffusion of two species, so that the third species could be treated as immobile. For the reaction forsterite + quartz = enstatite, the rate controlling diffusing components then would be MgO or SiO_2 or Mg_2Si_{-1} implying either coupled diffusion of Mg plus O, or Si plus O, or counter-diffusion of Mg plus Si (see also Yund 1997). It is also possible that the rate-limiting diffusion process involves the mobility of all species, implying counter-diffusion of MgO and SiO_2. It is clear that the rate-limiting diffusion process must be examined with respect to the volume proportions of replaced and produced phases.

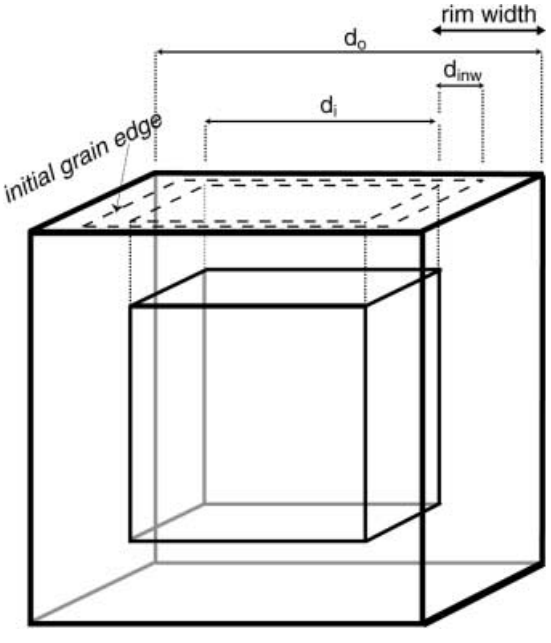

Fig. 3 Sketch showing an idealised cubic-shaped forsterite crystal that is replaced and overgrown by an enstatite rim. The rim advances in both inward and outward directions (see text). The inwards and outwards grown proportions are calculated with Eq. (3). d_o Width of remaining forsterite grain plus enstatite rim; d_i width of remaining forsterite grain; d_{inw} inwards grown proportion of enstatite rim

If the MgO component migrates much faster than the SiO_2 component, Mg plus O would diffuse from the forsterite–enstatite interface to the enstatite–quartz interface. In this case, the two partial reactions occurring at opposite sides of the rim are (migrating components in italics)

$$Mg_2SiO_4 = 0.5\ Mg_2Si_2O_6 + MgO \quad (5)$$

at the forsterite–enstatite interface, and

$$MgO + SiO_2 = 0.5\ Mg_2Si_2O_6 \quad (6)$$

at the enstatite–quartz interface. The less mobile SiO_2 does not appear as a mobile component in either of these interface reactions. In this case diffusion of the MgO component would be rate controlling. Because equal amounts of enstatite would be produced at the two interfaces, the position of the initial interface would be in the middle of the enstatite rims (Fig. 4a).

If the SiO_2 component migrates faster than the MgO component, Si and O must diffuse from the enstatite–quartz interface to the forsterite–enstatite interface. As pointed out above, the available space for the partial reaction at the forsterite–enstatite interface is restricted to the volume of the replaced forsterite. Thus, enstatite formation by fast SiO_2 diffusion to the forsterite–enstatite interface additionally requires outward diffusion of MgO. If the reacted forsterite is totally replaced by enstatite, the reaction at the forsterite–enstatite interface is

$$Mg_2SiO_4 + 0.38\ SiO_2 = 0.69\ Mg_2Si_2O_6 + 0.62\ MgO \quad (7)$$

The balanced reaction at the enstatite–quartz interface is then

$$0.62\ MgO + 0.62\ SiO_2 = 0.31\ Mg_2Si_2O_6 \quad (8)$$

Because of the constant-volume replacement of forsterite by enstatite, the position of the initial forsterite–quartz interface can be calculated with Eq. (3) (Fig. 4b). The rate-limiting diffusion process would be the outward diffusion of MgO.

A special situation would occur if MgO were to be slightly more mobile than SiO_2. In this situation, SiO_2 could be too slow to provide constant-volume replacement of forsterite, but too fast to be treated as immobile. In this special case at the forsterite–enstatite interface any intermediate reaction between (5) and (7) could occur; accordingly, at the enstatite–quartz interface, any intermediate reaction between (6) and (8) would emerge.

If both Mg and Si migrate faster than oxygen, enstatite would grow by counter-diffusion of Mg plus Si (i.e. diffusion of the Mg_2Si_{-1} component). The partial reactions at the two interfaces would then be

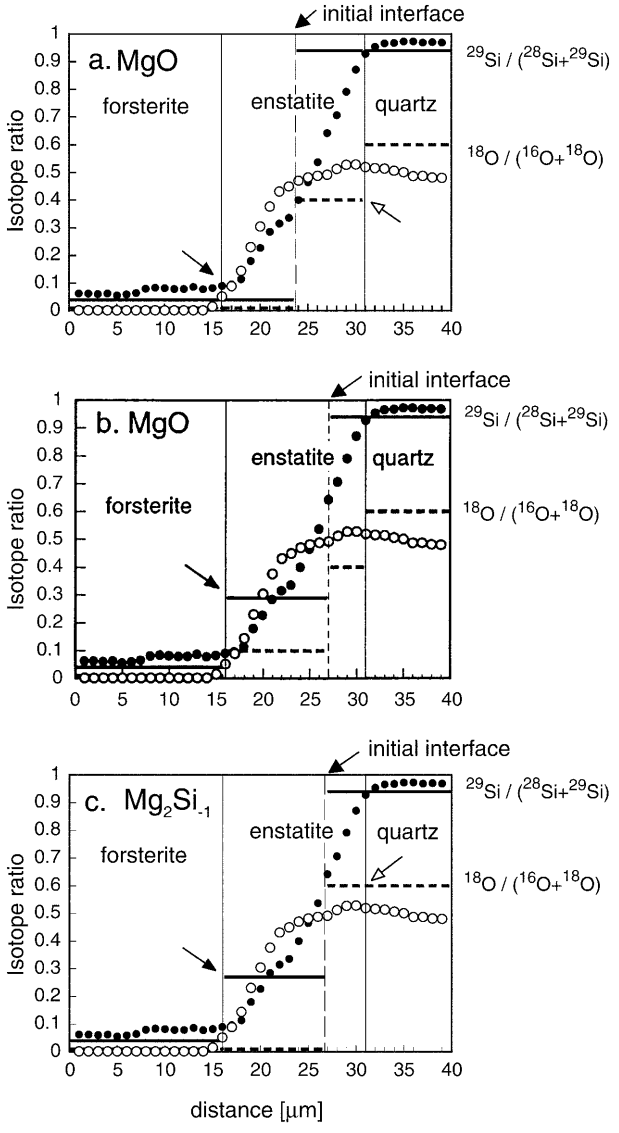

Fig. 4 Predicted isotope concentration profiles across the rim assuming that only interface reactions affect the isotopic composition of the enstatite (i.e., neither interdiffusion within the rim nor isotope exchange with the reactants occurred). The *thick black lines* show $^{29}Si/(^{28}Si + {}^{29}Si)$ in the enstatite rim and the initial values in the reactants. The *dashed lines* show $^{18}O/(^{18}O + {}^{16}O)$ in enstatite and the reactants. Superimposed are the measured isotopic data from Fig. 2a. See text for explanation of arrows. **a** Model assuming that MgO is the most mobile component, MgO diffusion is rate-limiting and the process is controlled by boundary reactions (5) and (6). For Si isotopes, a sharp concentration step occurs at the initial forsterite–quartz interface (*thick black lines*). For O isotopes, two steps are predicted, one at the initial forsterite–quartz interface and one at the enstatite–quartz interface (*thick dashes*). **b** Model assuming that SiO_2 is the most mobile component, MgO diffusion is rate-limiting and the process is controlled by boundary reactions (7) and (8). The position of the initial interface is calculated by Eq. (3). For Si isotopes, concentration steps occur at the initial interface and at the forsterite–enstatite interface (*thick black lines*). For O isotopes, concentration steps are predicted on the initial forsterite–quartz interface and the forsterite–enstatite and enstatite–quartz interfaces (*thick dashes*). **c** Model assuming that counter-diffusion of Mg_2Si_{-1} is rate-limiting, and boundary reactions (9) and (10) control the process. For Si isotopes, two steps are predicted to occur here, one at the forsterite–enstatite boundary and one at the initial forsterite–quartz boundary. For O isotopes, only one step would form at the initial interface. For further explanation see text

$$3\,Mg_2SiO_4 + Si = 2\,Mg_2Si_2O_6 + 2\,Mg \quad (9)$$

at the forsterite–enstatite interface, and

$$2\,Mg + 3\,SiO_2 = Mg_2Si_2O_6 + Si \quad (10)$$

at the enstatite–quartz interface.

At the forsterite–enstatite interface, 2 mol of enstatite would be formed at the expense of 3 mol forsterite. Thus, there are no volumetric impediments that would prevent reactions (9) and (10) at the two interfaces (Fig. 4c). Here, the slower of the two cations would be rate controlling.

Therefore, we predict that the rate of our reaction is either controlled by diffusion of the MgO component or, if counter-diffusion of Mg plus Si is operating, by the slower of these two cations. According to this argument, it is not possible that the diffusion of the SiO_2 component controls the rate of rim growth. Evaluation of our isotope profiles give crucial additional constraints on the rate-limiting process.

Identifying the rate-limiting component from the isotope profiles

We have shown that enstatite rim growth takes place from the initial forsterite–quartz interface towards both sides and we have defined the partial reactions that might be occurring at the forsterite–enstatite and enstatite–quartz interfaces. If MgO diffusion is rate-limiting, enstatite forms by reactions (5) and (6) or (7) and (8), if counter-diffusion of the Mg_2Si_{-1} component is rate-limiting, enstatite forms by reactions (9) and (10). Clearly the respective interface reactions will uniquely establish the isotopic composition of enstatite at either side.

Using the stoichiometric relationships between the interface reactions, the isotopic composition of enstatite growing in either direction can be calculated in terms of isotopic mass balance. As a first step, two simplifying assumptions are necessary: (1) the reaction boundaries at the forsterite–enstatite and enstatite–quartz interfaces are closed to isotopic exchange, and (2) there is no concomitant homogenisation of Si and O isotopes within the rim. It is clear that the measured profiles are not consistent with these assumptions. We have already established that quartz was open to oxygen exchange with the enstatite rim and that a smoothing of the profiles because of self-diffusion is realistic. However, the interface reactions still control the isotopic composition at the boundaries, and simple isotopic mass balance allows the identification of the rate-controlling diffusing component. Because of these simplifying assumptions the mass balance calculations predict sharp steps in the isotopic profiles at the respective interfaces, as well as at the initial forsterite–quartz boundary (thick lines in Fig. 4a–c).

Figure 4a shows the predicted sharp steps in isotope composition based on the model that MgO is more mobile than SiO_2 such that MgO diffusion is rate-controlling. The inwards grown enstatite formed by Eq. (5) inherits the isotopic composition of both Si and O isotopes from the forsterite. The outwards grown enstatite formed by Eq. (6) inherits its Si isotopic composition from the quartz, and its O isotopic composition is the product of two-thirds from quartz and one-third MgO component derived from the forsterite. Figure 4b shows the predicted steps if SiO_2 is more mobile than MgO. The inwards grown enstatite formed by Eq. (7) inherits its Si isotopic composition by 72% contribution of forsterite and 28% contribution of quartz, and its O isotope composition by 84% contribution of forsterite and 16% contribution of quartz. The outward grown enstatite formed by Eq. (8) inherits its Si isotope composition from the quartz and its O isotope composition from one-third contribution of forsterite and two-thirds contribution of quartz. Figure 4c shows the predicted sharp steps if counter-diffusion of the Mg_2Si_{-1} component is rate-limiting. The inwards grown enstatite formed by Eq. (9) inherits its O isotope concentration from the forsterite, and its isotopic composition of Si is the product of three-quarters from forsterite and one-quarter from quartz. In this case, the outwards grown enstatite formed by Eq. (10) would inherit both Si and O isotopes from the quartz.

Our three models make distinct and testable predictions: if MgO is the most mobile component, then the enstatite at the forsterite–enstatite interface would not see Si from quartz (black arrow in Fig. 4a) and the enstatite at the enstatite–quartz interface would see oxygen from the forsterite (white arrow in Fig. 4a). In contrast, if SiO_2 is more mobile than MgO, the enstatite at the forsterite–enstatite interface would see Si from the quartz (black arrow in Fig. 4b) and the enstatite at the enstatite–quartz interface would see O from the forsterite (white arrow in Fig. 4b). Finally, if counter-diffusion of the Mg_2Si_{-1} component is rate-limiting, the enstatite at the forsterite–enstatite interface would see Si from quartz (black arrow in Fig. 4c) and the enstatite at the enstatite–quartz interface would not see oxygen from forsterite (white arrow in Fig. 4c). Figure 4a–c also shows the measured isotope concentration profiles adapted from Fig. 2a. It is obvious that the enstatite did not incorporate any Si from the quartz at the forsterite–enstatite interface. Equally clear is that that the enstatite at the enstatite–quartz interface did incorporate O from the forsterite. We therefore conclude that MgO is more mobile than SiO_2 and that MgO diffusion controls the rate of rim growth. Smoothing of the concentration profiles does not invalidate this conclusion. The simplified model for MgO diffusion at closed boundaries predicts that the oxygen isotope ratio should be 0.4 at the enstatite–quartz interface. The actual value is about 0.5 (white arrow in Fig. 4a), which can easily be explained by an additional exchange of oxygen between the enstatite and quartz. In other words, the enstatite–quartz boundary was open to O exchange and even the quartz incorporated light oxygen from the forsterite. The scenario in Fig. 4a is the only model that is in accordance with the measured isotope profiles. The absence of Si from the quartz at the forsterite–enstatite interface rules out that SiO_2 is more mobile than MgO. None of the characteristics of the measured isotope profiles can be explained by a counter-diffusion of Mg_2Si_{-1} as the rate-controlling component.

Additionally, our conclusion is supported by the enrichment of fluid inclusions at the forsterite–enstatite interface in experiment FQ002 with added water (Fig. 1b). The water is initially distributed within the quartz matrix and diffuses to the forsterite–enstatite interface during rim growth. Thus, the rims tend to grow away from the forsterite grains and create open space as predicted by fast outward diffusion of MgO, but are held back by the confining pressure.

Unravelling the diffusion profiles

We have shown that the isotopic composition of enstatite at the enstatite–forsterite and enstatite–quartz interfaces requires that MgO is the rate-controlling component. The isotopic composition of the enstatite at the boundaries is controlled by the two interface reactions. However, the interface reactions alone do not explain the measured shapes of the diffusion profiles. In principle, these shapes developed during a complex interplay of three processes: (1) the propagation of the two interfaces controlled by MgO diffusion, (2) the homogenisation of the isotope concentrations by grain boundary self-diffusion of both Si and O within the rim, and (3) the isotope exchange across the enstatite–forsterite and enstatite–quartz interfaces. Because the grain sizes of both reactants, forsterite and quartz, are large relative to the micron-sized enstatite within the rim, significant diffusion across the rim boundaries requires sufficiently fast volume diffusion rates for O and Si within the reactants. It can be reasonably assumed that grain boundary diffusion rates of O and Si within the enstatite rim are much faster than their volume diffusion rates in quartz and forsterite. The rate of isotopic exchange across the boundaries must have been controlled by the volume diffusion rates within the initial reactants (i.e. how fast isotopes from the interior parts of the reactant grains could be supplied for exchange at the interface). Below we examine the influence of each of these three processes on the resulting profiles.

The silicon profile

The observed isotope ratios at the interfaces indicate that there is virtually no silicon exchange across the propagating reaction boundaries. This is also supported by the fact that, within our spatial resolution of 2 μm, the distribution of ^{28}Si and ^{29}Si in the outer and inner

zone of the enstatite rim is symmetric. Minor discrepancies result from the irregular enstatite–quartz interface (Fig. 1a). The constant gradient in $^{29}Si/(^{28}Si + ^{29}Si)$ ratio across the rim requires that the propagation of the interfaces, controlled by MgO diffusion, is faster than the homogenization of Si isotopes through self-diffusion behind the advancing fronts. Were MgO diffusion the sole diffusion mechanism within the enstatite, then a step in isotope composition at the initial forsterite–quartz boundary would have been preserved. This is not the case. Still, the isotope ratios of enstatite at the two interfaces are pinned to those of the reactants and are therefore constant through any time. Having established that the Si isotope compositions are fixed at the interfaces, it is possible to calculate grain boundary diffusion coefficients for Si within the enstatite matrix.

The Si isotope profile results from diffusion along enstatite grain boundaries plus an amount of volume diffusion out of the boundaries into the enstatite cores, classified as type B kinetics regime (Harrison 1961). For the regime of type B kinetics, the product of the grain boundary diffusion coefficient (D') and the effective grain boundary width (δ) is calculated using the relation of LeClaire (1963) as derived from the constant source solution of Whipple (1954; see also Joesten 1991):

$$D'\delta = \left(\frac{\partial \ln c}{\partial y^{6/5}}\right)^{-5/3} \left(\frac{4D}{t}\right)^{1/2} (0.661) \qquad (11)$$

where c is the measured Si isotope composition at the distance y from the initial interface, D is the volume diffusion coefficient of Si in enstatite, and t the run duration. Equation (11) requires constant compositions at both ends of the diffusion profile at any time, which we have established for our data set.

With Eq. (11), a plot of ln $c(^{29}Si)$ versus $y^{6/5}$ should result in a straight line. This is shown in Fig. 5a for the ^{29}Si isotope concentrations from Fig. 2a, using only values from the section within the enstatite rim. For the calculation of $D'\delta$ for Si, values of the volume diffusion coefficient D_{Si} in enstatite are required. To our knowledge, there are no data published on $D^{Vol}_{Si,En}$. It can, however, reasonably be assumed that Si diffusion in orthopyroxene is similar to that of clinopyroxene. If so, we can use $D^{Vol}_{Si,Di}$ in diopside measured between 1,250 and 1,040 °C at 1 bar under almost dry conditions (Béjina and Jaoul 1996). Extrapolated to 1,000 °C, their data yielded a value for $D^{Vol}_{Si,Di}$ of 5×10^{-23} m^2 s^{-1}. With this, and the slope derived from Fig. 5a, we calculate $\acute{D}_{Si,En}\delta$ at 1,000 °C to be 3×10^{-24} m^3 s^{-1}. The major uncertainty in this calculation comes from the estimation of $D^{Vol}_{Si,Di}$ because the water fugacity might have been different from our experiments and it is not clear how this would affect silicon diffusion in enstatite. It is known that the presence of water enhances volume diffusion rates in silicates (Freer 1993) – from dry to water saturated conditions volume diffusion coefficients may increase by several orders of magnitude. If we tentatively assume that $D^{Vol}_{Si,Di}$ and $D^{Vol}_{Si,En}$ are similarly increased by three orders of magnitude in the presence of traces of water and at 1 GPa confining pressure, then the calculated value for $\acute{D}_{Si}\delta$ at 1,000 °C would increase to $\sim10^{-22}$ m^3 s^{-1}.

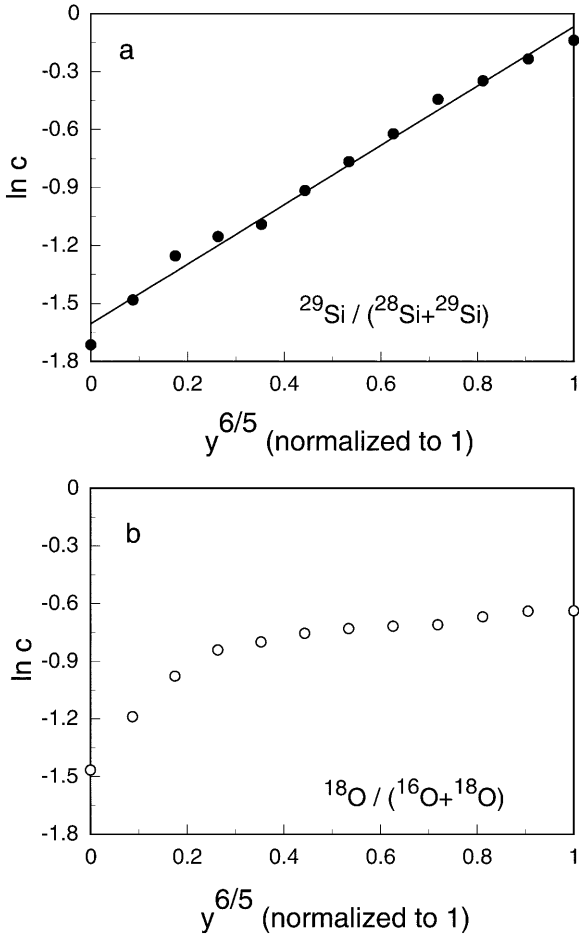

Fig. 5a, b Plots of ln $c(^{29}Si)$ versus $y^{6/5}$ normalised to 1, according to Eq. (11). **a** $^{29}Si/(^{28}Si + ^{29}Si)$; **b** $^{18}O/(^{16}O + ^{18}O)$. Values are taken from Fig. 2b, and refer only to those SIMS data collected from within the enstatite rim. Ratios for Si are approximated by a *straight line* generated by the inter-diffusion of Si isotopes. Data for O do not plot on a straight line due to oxygen's open system behaviour with respect to quartz

For Si, we observed isotopic exchange with the reactants across neither the forsterite–enstatite nor across the enstatite–quartz interfaces. This can be explained in terms of measured volume diffusion coefficients $D^{Vol}_{Si,Fo}$ and $D^{Vol}_{Si,Qz}$ from the literature applied to the equation for transport normal to the surface of a semi-infinite volume (Crank 1975):

$$\frac{C_x - C_1}{C_0 - C_1} = erf\frac{x}{2\sqrt{Dt}} \qquad (12)$$

where C_x = Si isotope concentration at distance x; C_1 = concentration at the interface; C_0 = initial concentration of the reactants; D = volume diffusion coefficient; t = run duration. Inserting isotope compositions into Eq. (12) reveals that $D^{Vol}_{Si,qtz}$ must exceed 10^{-17} m^2 s^{-1} to allow significant influx of ^{28}Si into the quartz, and ^{29}Si into the rim, respectively. Similarly, loss or gain of Si isotopes across the forsterite–enstatite interface would

require $D^{vol}_{Si,fo} > 10^{-17}$ m^2 s^{-1}. Above 1,000 °C, $D^{Vol}_{Si,qtz}$ were determined by Béjina and Jaoul (1996) in dry and pure quartz at 0.1 MPa in air. Extrapolated to 1,000 °C, their data give $D^{Vol}_{Si,qtz} = 7 \times 10^{-28}$ m^2 s^{-1}. To our knowledge, there are no experimentally determined values available for $D^{Vol}_{Si,qtz}$ under hydrothermal conditions. The effect of additional water may be roughly estimated from NaSi–CaAl interdiffusion rates in feldspars. At 1,500 MPa, interdiffusion coefficients are about three orders of magnitude larger in 'wet' experiments as compared with dry conditions (Grove et al. 1984; Liu and Yund 1992). Values for $D^{Vol}_{Si,Fo}$ were determined by Jaoul et al. (1981) and Andersson et al. (1989) also above 1,000 °C. Extrapolation to 1,000 °C yields values of $D^{Vol}_{Si,Fo}$ in the range of 10^{-25} to 10^{-26} m^2 s^{-1}, again far off the required 10^{-17} m^2 s^{-1} for exchange across the interface. It is clear that volume diffusion of Si in both reactants, dry or wet, is not fast enough to allow significant Si exchange. This confirms our observation that the forsterite–enstatite and enstatite–quartz interfaces remained closed to Si exchange and that complete mass balance of Si isotopes within the rim was achieved.

The oxygen profile

The oxygen isotope compositions at the interfaces indicate that there was no significant exchange across the advancing forsterite–enstatite interface. This was not true for oxygen exchange at the enstatite–quartz interface. There is significant depletion of heavy oxygen in quartz that corresponds with an excess of heavy oxygen within the rim. A flat profile of $^{18}O/(^{16}O + ^{18}O)$ developed from inside the quartz across the enstatite–quartz interface and extended even beyond the initial forsterite–quartz boundary. Towards the forsterite interface, $^{18}O/(^{16}O + ^{18}O)$ drops continuously resulting in a significantly steeper limb of the profile. The boundary reactions derived for MgO diffusion in a closed system predict a $^{18}O/(^{16}O + ^{18}O)$ gradient at the enstatite–quartz interface and no gradient at the forsterite–enstatite interface. Therefore, exchange of oxygen only shifts $^{18}O/(^{16}O + ^{18}O)$ ratios at either side of the enstatite–quartz interface. The $^{18}O/(^{16}O + ^{18}O)$ ratios at either side of the forsterite–enstatite interface remain unchanged.

We have shown that there is only one Si-transporting mechanism acting within the rim, namely grain boundary interdiffusion across the initial forsterite–quartz interface. In contrast, the oxygen isotope profile results from a combination of three O-transporting processes: MgO transports ^{16}O from forsterite to the enstatite–quartz interface; exchange of ^{16}O and ^{18}O occurs between enstatite and quartz across this interface; and ^{16}O and ^{18}O homogenise by interdiffusion at the initial forsterite–quartz interface behind the advancing front, as did Si. The measured oxygen profile is therefore complex. In contrast to Si, a simple inter-diffusion profile is not seen because ^{18}O influx from quartz overprints the homogenisation at the initial forsterite–quartz interface. The two different diffusion processes, oxygen inter-diffusion across the initial interface and ^{18}O influx from the quartz, overlap. Both mechanisms proceeded across different concentration gradients, and we cannot define stable boundary conditions for either process. This is also seen in a plot of ln $c(^{18}O)$ versus $y^{6/5}$ (Fig. 5b). The oxygen isotope profile is not approximated by a straight line and we cannot apply Eq. (11) because the precondition of fixed boundary conditions is not achieved. Therefore, we cannot derive reliable values for $\acute{D}_{Ox,En}\delta$ from our experiments.

Oxygen isotopic exchange across the enstatite–quartz interface can be interpreted in terms of volume diffusion coefficients $D^{Vol}_{Ox,Qz}$ from the literature. Values of $D^{Vol}_{Ox,Qz}$ in β-quartz at dry conditions are in the range of 10^{-20} to 10^{-22} m^2 s^{-1} (Joesten 1991). Values are significantly increased under hydrothermal conditions and, extrapolated to 1,000 °C, fall in a small range of 3×10^{-17} m^2 s^{-1} to 6×10^{-17} m^2 s^{-1} at 100 MPa (Dennis 1984; Giletti and Yund 1984; Elphick et al. 1986). Thus the oxygen diffusion coefficient is a function of the water fugacity (Farver and Yund 1991). Because our experiments are not water saturated, the water fugacity is unknown. However, at 1,000 MPa a diffusion coefficient $D^{vol}_{O,qtz} > 10^{-17}$ m^2 s^{-1} as required for ^{18}O influx seems realistic. If so, volume diffusion of oxygen in quartz would be fast enough to allow significant oxygen exchange between enstatite and quartz. This is confirmed by our observation that the enstatite–quartz interface is open to oxygen exchange and that oxygen isotope distribution within the rim continued to evolve with time. One may speculate about why the $^{18}O/(^{16}O + ^{18}O)$ ratio in quartz shows a constant value of 0.52 along a distance of 10 μm from the enstatite–quartz interface. This is easily explained by presence of large enstatite crystals intergrown with quartz grains, which points to significant quartz recrystallisation at that interface. It is clear that quartz recrystallisation would enhance oxygen isotope transport.

Values for $D^{Vol}_{Ox,Fo}$ in forsterite have been determined under dry conditions or very low H_2O fugacities at different temperatures and 0.1 MPa (Reddy et al. 1980; Hallwig et al. 1982; Jaoul et al. 1983). Extrapolation to 1,000 °C yields a range of values between 2×10^{-22} m^2 s^{-1} and 5×10^{-24} m^2 s^{-1}. These values are roughly one order of magnitude lower than oxygen diffusion coefficients in dry quartz. Assuming that water affects oxygen diffusion in forsterite to a similar degree as in quartz, the oxygen mobility in forsterite should also be about one order of magnitude lower than in quartz. This would only allow very limited oxygen exchange across the forsterite–enstatite boundary. If such is the case, then this effect was below the spatial resolution of our method.

Comparison with other grain boundary diffusion measurements

We have shown that our model, based on a mass-conserving reference frame including rim growth to both

sides of the initial interface, explains both the formation of the enstatite rims and the resulting isotope profiles. The main conclusion is that MgO diffusion controls the rate of the rim growth.

Using our synthetic forsterite, we conducted two experiments of different run durations that resulted in different rim widths (Table 1). In an χ^2 versus t-plot, the two data points plus the origin are approximated by a straight line with the slope of 8.2 $\mu m^2\ h^{-1}$ (Fig. 6). Using Eq. (1) the grain boundary diffusivity of MgO in enstatite, $\acute{D}_{MgO}\delta$, can be calculated. Eq. (1) relates the rim growth rate to the driving force derived from the difference in the chemical potentials of MgO at the two reaction boundaries. Assuming local equilibrium was established at both the forsterite–enstatite and the enstatite–quartz interfaces, the gradient in the chemical potentials of MgO at either side is related to the Gibbs free energy of the overall reaction (see also Yund 1997).

$$\Delta\mu_{MgO}^{Fo/En/Qz} = \mu_{MgO}^{Fo/En} - \mu_{MgO}^{En/Qz} = G_{Fo}^{P,T} + G_{Qz}^{P,T} - G_{En}^{P,T} = -\Delta G_R \qquad (13)$$

Inserting $\Delta G_R = -9.6$ kJ mol^{-1} (Holland and Powell 1990) into Eq. (1) reveals that $\acute{D}_{MgO}\delta$ is $\sim 8 \times 10^{-22}\ m^3\ s^{-1}$ at 1,000 °C and 1 GPa for the iron-free system. Figure 6 also shows our measured x2 versus t values for experiments using San Carlos olivine as reactant. It is clear that under identical conditions the thinner reaction rims indicate a lower MgO (+FeO) diffusivity compared with the iron-free system. As a result, values of $\acute{D}_{MgO}\delta$ in the iron-bearing system are estimated to be lower by about a factor of five under nominally dry conditions, and by a factor of two if 0.4 wt% water is present.

The growth rates of enstatite rims produced by reaction of olivine (fo_{92}) and SiO_2 were experimentally examined by Yund (1997) at varying conditions of 250–1,500 MPa, 900–1,100 °C, and a wide range of water contents. For comparison, Fig. 6 also shows Yund's (1997) χ^2 versus t curves for 1,000 °C at both 700 MPa and 1,400 MPa, and different amounts of water present. Rates depend significantly on both pressure and water contents: increasing pressure from 700 to 1,400 MPa enhances rates by a factor of ~4, as does the addition of water. The important point is that these rim growth rates are similar to ours where, for our experiments with San Carlos olivine, a rate enhancement from nominally dry to wet conditions by a factor of three is also indicated. Our rates at 1,000 °C, 1,000 MPa and nominally dry conditions for iron-free forsterite coincide with that for fo_{92} at 1,400 MPa and 0.1 wt% H_2O (Yund 1997). Although the effects of iron content, pressure and water contents are not understood in detail, similar rates are observed and it can reasonably be assumed that the same rate-limiting process determined the overall rim growth over a broad parameter space. Yund (1997) interpreted his measured rim growth rates alternatively in terms of MgO, SiO_2 or Mg_2Si_{-1} diffusion and derived possible values for $\acute{D}_{MgO}\delta$, $\acute{D}'_{SiO_2}\delta$ and $\acute{D}'_{Mg_2Si_{-1}}\delta$ assuming in turn that the respective component was rate-limiting. Based on our above reasoning, it would appear that his values for $\acute{D}_{MgO}\delta$ were the correct choice.

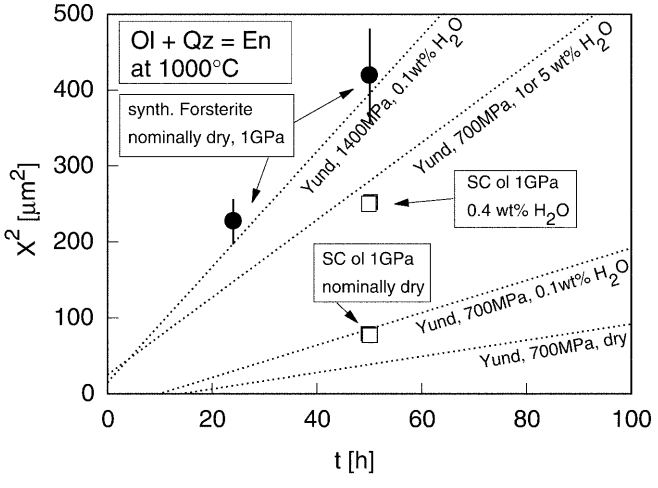

Fig. 6 Enstatite rim widths raised to the 2nd power (μm^2) versus *t* (h) with iron-free forsterite (*filled circles*) and San Carlos olivine (*open squares*; values from Table 1) along with x^2 versus t curves for fo_{92} at 1,000 °C, 700 and 1,400 MPa, and different water contents (*dashed lines*; Yund 1997)

Figure 7 shows an Arrhenius diagram for different components and different minerals from the literature along with our data for $\acute{D}_{MgO}\delta$ and $\acute{D}_{Si}\delta$ in enstatite. Our value for $\acute{D}_{MgO}\delta$ at 1,000 °C in iron-free enstatite is about $8 \times 10^{-22}\ m^3\ s^{-1}$. This value is significantly lower for rims formed around iron-bearing San Carlos olivine. In any case, these MgO diffusivities are in close agreement with those measured by Yund (1997) between 900 and 1,100 °C. Based on our conclusions above, our value for $\acute{D}_{Si}\delta$ at 1,000 °C in iron-free enstatite is $3 \times 10^{-24}\ m^3\ s^{-1}$ calculated with $D_{Si,Di}^{Vol}$ for dry conditions, and about $10^{-22}\ m^3\ s^{-1}$ for wet conditions. Aside from this, experimentally determined grain boundary diffusivities of Si are only known in nearly dry and wet quartz (Farver and Yund 2000). At 1,000 °C, $\acute{D}_{Si,Oz}\delta$ are in the range of $10^{-21}\ m^3\ s^{-1}$ for wet, and about 5 times lower for nearly dry quartz. Thus, grain boundary diffusivities of Si in enstatite are lower by circa one order of magnitude as compared to quartz.

Growth rates of enstatite rims between powdered San Carlos olivine and quartz grains have been determined by Fisler et al. (1997) at 1,350 to 1,450 °C and 0.1 MPa under dry conditions at various oxygen fugacities. Here, rim growth was interpreted as controlled by grain boundary diffusion of SiO_2 through the enstatite rim. The resulting SiO_2 diffusivities are in the range of $10^{-21}\ m^3\ s^{-1}$ at these high temperatures (Fig. 7). These results are difficult to compare with ours because pressure and temperature were completely different and the rate-controlling process might be radically different if water is absent.

Concluding remarks

A striking point is that enstatite rims around iron-free forsterite grew significantly faster than around San

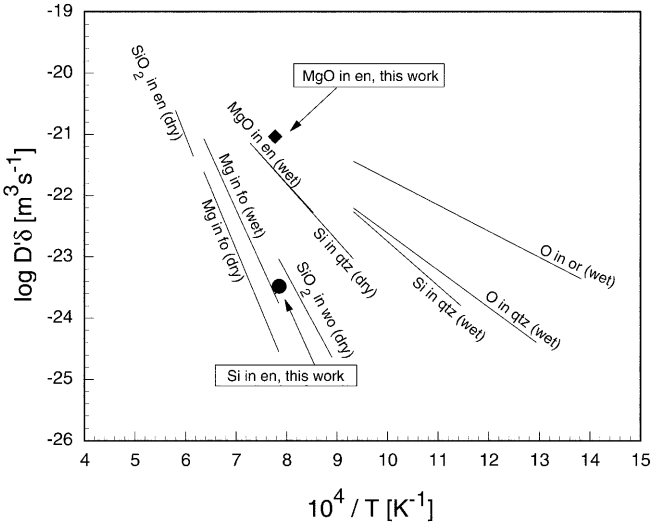

Fig. 7 Arrhenius plot of experimentally determined grain boundary diffusivities for different components and different minerals from the literature involving Mg, O and Si, as well as MgO and SiO_2 along with our data for $\acute{D}_{MgO}\delta$ and $\acute{D}_{Si}\delta$ in enstatite. Values for O in orthoclase are from Farver and Yund (1995a) and in quartz from Farver and Yund (1991) both at 100 MPa water pressure. Values for Si in wet and dry quartz are from Farver and Yund (2000). Mg in wet and dry forsterite is from Farver et al. (1994). MgO in enstatite is at 700 MPa and 0.1 wt% water (Yund 1997). SiO_2 in wollastonite at 100 MPa CO_2 pressure is from Milke and Heinrich (2000), and SiO_2 in dry enstatite is from Fisler et al. (1997)

Carlos olivine. Given that grain boundary diffusion of MgO is rate-controlling and that the same boundary reactions (4) and (5) also occurred for the FeO component, it would appear that the presence of even modest amounts of FeO within the rim hampered the reaction progress. One may speculate that MgO and FeO travelled at different rates through the developing rim. If so, one could imagine that FeO along grain boundaries inhibits fast MgO diffusion. The mechanism of that remains unknown and further study will be required (e.g. by detailed investigation of the grain boundaries by analytical transmission electron microscopy). It is also possible that the defect structure of pure and iron-bearing enstatite is different because of the oxidation state of Fe. At given redox conditions pure and iron-bearing enstatite may have completely different vacancy concentrations, both in volume and along grain boundaries.

Our study points out that the growth of enstatite rims between forsterite and quartz is best described by a constant-mass reference frame, and not by a volume-conserving frame. This involves rim growth in both directions irrespective of which migrating component is rate-controlling. The initial interface is therefore always located within the reaction rim. Many experiments have attempted to preserve the position of the initial interface with inert markers, e.g. Pt paint (Brindley and Hayami 1965; Schmalzried 1978; Fisler and Mackwell 1994; Fisler et al. 1997; Yund 1997). Growth in both directions away from an inert marker has often been interpreted as indicating counter-diffusion as the rate-controlling process. Our isotope tracer experiment has shown that this interpretation is wrong. The enstatite rims grew in both directions although the rate-limiting process was directional MgO grain boundary diffusion and not counter-diffusion. This is aside from any possible errors that could result from the migration of apparently inert markers with advancing reaction interfaces.

It is clear that inert marker experiments can only be evaluated if the position of the initial interface is considered based on the volumes of reaction products and consumed reactants. The rim growth to both sides from the initial interface is limited by the available space and by the relative migration rates of the diffusing species. The diffusion rates of different species may react differently to modified reaction conditions. For example, in contact metamorphic marbles wollastonite rims typically overgrow quartz nodules (Joesten and Fisher 1988; Heinrich et al. 1995). From hydrothermal experiments (Kridelbaugh 1973; Tanner et al. 1988; Milke and Heinrich 2000) it is well known that wollastonite rims produced by the reaction calcite + quartz = wollastonite + CO_2 replace quartz under H_2O absent conditions, and replace calcite if a H_2O–CO_2 fluid is present. Minor variations in the growth conditions can therefore significantly alter the evolution of diffusion-controlled reaction rims.

Acknowledgements We thank F. Wallrafen (Bonn) for providing synthetic forsterite and K. Simon (Göttingen) for analysing our quartz reactant for oxygen isotopes. E.M. Schemmert made the sample mounts and U. Glenz provided SEM facilities, which are gratefully acknowledged. We wish to thank A. Dimanov and R. Abart for helpful comments.

References

Andersson K, Borchardt G, Scherrer S, Weber S (1989) Self-diffusion in Mg_2SiO_4 (forsterite) at high temperature. Fresenius Z Anal Chem 333:383–385

Béjina F, Jaoul O (1996) Silicon self-diffusion in quartz and diopside measured by nuclear micro-analysis methods. Phys Earth Planet Int 97:145–162

Berner RA (1978) Rate control of mineral dissolution under earth surface conditions. Am J Sci 278:1235–1252

Brady JB (1983) Intergranular diffusion in metamorphic rocks. Am J Sci 283A:181–200

Brindley GW, Hayami R (1965) Kinetics and mechanism of formation of forsterite (Mg_2SiO_4) by solid state reaction of MgO and SiO_2. Philos Mag 12:505–514

Crank J (1975) The mathematics of diffusion, 2nd edn. Oxford University Press, Oxford

Dennis PF (1984) Oxygen self-diffusion in quartz under hydrothermal conditions. J Geophys Res 89:4047–4057

Dimanov A, Jaoul O, Sautter V (1996) Calcium self-diffusion in natural diopside single crystals. Geochim Cosmochim Acta 60:4095–4106

Edwards KJ, Valley JW (1998) Oxygen isotope diffusion and zoning in diopside; the importance of water fugacity during cooling. Geochim Cosmochim Acta 62:2265–2277

Elphick SC, Dennis PF, Graham CM (1986) An experimental study on the diffusion of oxygen in quartz and albite using an overgrowth technique. Contrib Mineral Petrol 92:322–330

Farver JR, Yund RA (1991) Oxygen diffusion in quartz: dependence on temperature and water fugacity. Chem Geol 90:55–70
Farver JR, Yund RA (1992) Oxygen diffusion in a fine-grained quartz aggregate with wetted and nonwetted microstructures. J Geophys Res 97:14017–14029
Farver JR, Yund RA (1995a) Grain boundary diffusion of oxygen, potassium and calcium in natural and hot-pressed feldspar aggregates. Contrib Mineral Petrol 118:340–355
Farver JR, Yund RA (1995b) Interphase boundary diffusion of oxygen and potassium in K-feldspar/quartz aggregates. Geochim Cosmochim Acta 59:3697–3705
Farver JR, Yund RA (1996) Volume and grain boundary diffusion of calcium in natural and hot-pressed calcite aggregates. Contrib Mineral Petrol 123:77–91
Farver JR, Yund RA (2000) Silicon diffusion in a natural quartz aggregate: constraints on solution-transfer diffusion creep. Tectonophysics 325:193–205
Farver JR, Yund RA, Rubie DC (1994) Magnesium grain boundary diffusion in forsterite aggregates at 1,000°–1,300 °C and 0.1 MPa to 10 GPa. J Geophys Res 99:19809–19819
Fisler DK, Mackwell SJ (1994) Kinetics of diffusion-controlled growth of fayalite. Phys Chem Mineral 21:156–165
Fisler DK, Mackwell SJ, Petsch S (1997) Grain boundary diffusion in enstatite. Phys Chem Mineral 24:264–273
Freer R (1993) Diffusion in silicate minerals. Defect Diffusion Forum 101–102:1–17
Giletti BB, Yund RA (1984) Oxygen diffusion in quartz. J Geophys Res 89:4039–4046
Grove TL, Baker MB, Kinzler RJ (1984) Coupled CaAl–NaSi diffusion in plagioclase feldspar: experiments and application to cooling rate speedometry. Geochim Cosmochim Acta 48:2113–2121
Hallwig D, Schachtner R, Sockel HG (1982) Diffusion of magnesium, silicon and oxygen in Mg_2SiO_4 and formation of the compound in the solid state. In: Dryek K, Habor J, Nowotry J (eds) Reactivity of solids. Proceedings of the 9th International Symposium on the Reactivity of Solids, Cracow, 1–6 Sept 1980, Polish Scientific Publications, Warszawa, pp 166–169
Harrison LG (1961) Influence of dislocations on diffusion kinetics in solids with particular reference to alkali halides. Trans Faraday Soc 57:1191–1199
Heinrich W, Hoffbauer R, Hubberten HW (1995) Contrasting fluid flow patterns at the Bufa del Diente contact metamorphic aureole, north-east Mexico: evidence from stable isotopes. Contrib Mineral Petrol 119:362–376
Holland TJB, Powell R (1990) An enlarged and updated internally consistent thermodynamic data set with uncertainties and correlations: the system K_2O–Na_2O–CaO–MgO–MnO–FeO–Fe_2O_3–Al_2O3–TiO_2–SiO_2–C–H_2–O_2. J Metamorph Geol 8: 89–124
Jaoul O, Poumellec M, Froidevaux C, Havette A (1981) Silicon diffusion in forsterite: a new constraint for understanding mantle deformation. In: Stacey FD Paterson MS, Nicholas A (eds) Anelasticity in the Earth. Geodynamics series, vol 4. American Geophysical Union, Washington, DC, and Geological Society of America, Boulder, pp 95–100
Jaoul O, Houlier B, Abel F (1983) Study of ^{18}O diffusion in magnesium orthosilicate by nuclear microanalysis. J Geophys Res 88:613–624
Joesten R (1991) Grain-boundary diffusion kinetics in silicate and oxide minerals. In: Ganguly J (ed) Diffusion, atomic ordering, and mass transport. Springer, Berlin Heidelberg New York, pp 345–395
Joesten J, Fisher GW (1988) Kinetics of diffusion-controlled mineral growth in the Christmas Mountains (Texas) contact aureole. Geol Soc Am Bull 100:714–732
Kridelbaugh SJ (1973) The kinetics of the reaction: calcite + quartz = wollastonite + carbon dioxide at elevated temperatures and pressures. Am J Sci 273:757–777
LeClaire AD (1963) The analysis of grain boundary diffusion measurements. J Appl Phys 14:351–356
Liu M, Yund RA (1992) NaSi–CaAl interdiffusion in plagioclase. Am Mineral 77:275–283
Liu M, Peterson J, Yund RA (1997) Diffusion-controlled growth of albite and pyroxene reaction rims. Contrib Mineral Petrol 126:217–223
Milke R, Heinrich W (2000) Experimental investigation on grain-boundary diffusion in wollastonite rims. J Conf Abs 5:71
Parks GA (1990) Surface energy and adsorption at mineral–water interfaces: an introduction. In: Hochella M Jr, White AF (eds) Mineral–water interface geochemistry. Mineral Soc Am Rev Mineral 23:133–175
Reddy KPR, Oh SM, Major LD Jr, Cooper AR (1980) Oxygen diffusion in forsterite. J Geophys Res 85:322–326
Schmalzried H (1978) Reactivity and point defects of double oxides with emphasis on simple silicates. Phys Chem Mineral 2:279–294
Tanner SB, Kerrick DM, Lasaga AC (1985) Experimental kinetic study of the reaction: calcite + quartz = wollastonite + carbon dioxide, from 1 to 3kbars and 500° to 850 °C. Am J Sci 285:577–620
Whipple RTP (1954) Concentration contours in grain boundary diffusion. Philos Mag 45:1225–1236
Yund RA (1997) Rates of grain boundary diffusion through enstatite and forsterite reaction rims. Contrib Mineral Petrol 126:224–236